Received: 13 September 2019 | Revised: 30 December 2019 | Accepted: 9 February 2020

DOI: 10.1002/aic.16945

AIChE JOURNAL

PARTICLE TECHNOLOGY AND FLUIDIZATION

Development of a virtual Couette rheometer for aerated granular material

Lyes Ait Ali Yahia[1] | Tobias Matthaeus Piepke[1,2] | Ross Barrett[1] | Ali Ozel[1] | Raffaella Ocone[1]

[1]School of Engineering and Physical Sciences, Heriot-Watt University, Edinburgh, EH144AS, UK

[2]Institut Thermo und Fluiddynamik, Ruhr-Universität Bochum, 44780, Bochum, Germany

Correspondence
Raffaella Ocone, School of Engineering and Physical Sciences, Heriot-Watt University, Edinburgh EH14 4AS, UK
Email: r.ocone@hw.ac.uk

Funding information
Engineering and Physical Sciences Research Council, Grant/Award Number: EP/N034066/1

Abstract

A novel rheometer to study the behavior of granular materials in an aerated bed of particles has been developed. The device, called the aerated bed virtual Couette rheometer, is shown to be able to measure the shear stresses in the quasi-static and in the intermediate flow regimes. To validate the instrument, a Newtonian fluid of known viscosity was first sheared. The device was then used for measuring the shear stress of nonaerated glass beads with three -3D printed cells of different sizes to validate the optimal radial position, r^*, where both shear rate and shear stress are independent of the cell radius. The results for the nonaerated glass beads displayed Coulomb behavior. The same behavior was observed when the bed was aerated. These experiments also showed that for a fixed shear rate the shear stress decreases as the aeration velocity, U. increases.

KEYWORDS

aerated bed, rheology, glass beads, granular materials, inertial number

1 | INTRODUCTION

Granular materials are widely produced and handled in the chemical and process industries.[1] Indeed, such materials can be found in powder-based unit operations such as granulation and drying; fluid catalytic cracking processes; coal gasification; fluidized beds. Consequently, understanding their flow behavior is of critical importance to help industrial practitioners handle and produce particulates in an efficient and less costly way.

Three regimes are generally observed in granular flow: the quasi-static (slow) regime, the inertial (rapid) regime, and the intermediate regime. The quasi-static regime, which can be described by plasticity models,[2,3] is characterized by the formation, rotation, and breakage of force chains. This regime has been extensively studied experimentally through a number of experimental techniques such as shear testers.[4-9] The inertial regime, where the kinetic theory[10,11] is usually adopted, is characterized by instantaneous and binary collisions; such behavior has been widely investigated in various experimental configurations such as fluidized beds.[12-16] The intermediate regime, which develops between the slow and rapid regimes, has become the subject of numerical and experimental studies. Jop et al.[17] proposed the following constitutive law that predicts the behavior of dense granular flows over the three regimes:

$$\mu(I) = \mu_s + (\mu_2 - \mu_s)/(I_0/I + 1) \text{ with } I = \dot{\gamma}\, d_p/(P/\rho)^{0.5} \quad (1)$$

where μ is the friction coefficient, I is the inertial number, I_0 is a model constant, μ_s and μ_2 are the friction coefficients at low and high I, respectively. I depends on the shear rate, $\dot{\gamma}$, on the particle diameter, d_p, and on the applied pressure, P. Equation (1) states that the friction coefficient of the granular material has a critical value, μ_s, at low shear rates and converges to a limiting value, μ_2, at high inertial numbers.

Such a flow behavior in the quasi-static regime was successfully modeled by Equation (1) in different flow configurations, such as

inclined planes, rotating drum and plane and annular shear flows,[18] where the friction coefficient, $\mu(I)$, is evaluated as the ratio of the shear stress, τ, to the applied pressure, P. Similarly, a static solid-like state in fluidized bed, where particles are aerated by gas velocity lower than the fluidization velocity, U_{mf}, falls into the quasi-static regime.[19,20] In the static aerated bed, the fluidization index, (FI), which is defined as the ratio of the pressure drop to the total weight of the system, is less than 0.9.[21,22]

The behavior of granular materials in the static aerated bed has been investigated in several studies. Klein et al.[19] developed an annular shear cell to shear a limestone powder (d_p < 15 μm) at various normal pressures and with shear velocity ranging from 0.07 to 4,200 mm/min. This device enabled the studied sample to be aerated from the bottom during the test. The results showed that, for a constant applied pressure and an FI lower than 0.7, the shear stresses obtained with and without aeration are similar. However, for FI higher than 0.7, the measured shear stress under aeration decreases while increasing the air velocity following the intermediate behavior described by Equation (1). Barletta et al.[20] built a rotational shear tester for aerated shear flow by modifying the Peschl shear tester[23] to investigate the impact of aeration on the flow behavior of two cohesive powders: silica (d_p = 7.6 μm) and magnesium carbonate (d_p = 3.5 μm). They performed experiments at low shear rates and normal pressure with aeration lower than the minimum fluidization conditions (FI < 0.7). Their results showed that the aeration does not have an impact on the friction coefficient of the studied materials indicating that, even when aerated, the powders are still in the quasi-static regime. Valvedre et al.[21] and Castellanos et al.[22] developed the Sevilla Powder tester[21] that allows measuring the tensile strength of fine cohesive powders at very small normal pressures in a fluidized bed. The tensile strength is considered as the fracture point where the pressure drop across the bed falls abruptly before reaching a steady value. A mechanically stirred fluidized-bed rheometer (FBR) was used by Bruni et al.[24] and Tomasetta et al.[25] to study the rheology of powders aerated below the fluidization threshold. Glass beads and silica powders with different fine contents were tested. The torque necessary to rotate a flat impeller immersed in a bed of aerated powders was measured for different impeller depths and aeration rates. Similarly, Salehi et al.[26] used the Anton Paar powder cell to measure the torque necessary to rotate a flat impeller in beds of glass beads, sand and alumina powders aerated between no aeration to the fluidization limit. The experimental results showed that the measured torques depend on the material tested, on the airflow rate applied, on the impeller depth, and on the height of the impeller blade.

A different experimental configuration, the coaxial cylinder viscometer, was also used in a number of studies to investigate the particles stress in aerated and fluidized beds.[4,9,16,26-31] Such a device is commonly used for liquids[32,33] and consists of a rotating inner cylinder, the so-called bob, and a static outer cylinder or cup; the material under investigation is placed in the annular gap between the two cylinders. The shear stress is then computed from the torque, T, needed to move the rotating cylinder through the material. This type of flow configuration was adopted by Anjaneyulu and Khakhar[4] to study an aerated bed of glass beads with three different particle diameters (0.5, 0.7, and 0.9 mm). In those experiments, the air was injected from the bottom through the annular gap between the inner and outer cylinders. The experiments were performed with a small range of gas flowrates close to the minimum fluidization velocity, U_{mf}.

The results showed that when glass beads are aerated they behave as a Bingham fluid. The effective viscosity was found to level off to a nearly constant value when the flowrate increases above the minimum fluidization condition ($U > U_{mf}$, where U is the gas velocity), while the yield stress decreases monotonically. Both viscosity and yield stress were found to be nearly independent of the diameter of the particles when similar FI was maintained. Similarly, Colafigli et al.[16] evaluated the apparent viscosity of silica powders in the Couette FBR (CFBR), where they performed experiments above the minimum fluidization velocity. Their results revealed a pseudoplastic-type behavior and the apparent viscosities significantly decrease with increasing the shear stress. Landi et al.[29] used also the CFBR to investigate the flow properties of moisturized 48 mm glass beads with relative humidity ranging from 15 to 70%. The developed torques were measured below and above the minimum fluidization velocity. The results showed a steady and almost linear decrease of the torque through the whole fluidization process suggesting that the internal structure of the bed, even when fluidized, does not change significantly.[29] Tardos et al.[9] presented a study based on a device having similar Couette geometry where they investigated the solid bulk shear stress of a frictional aerated powder (glass beads and iron powder) using a slowly rotating rough cylinder. The authors performed experiments at low shear rates with U ranging from 0 to U_{mf}. One of the major findings of the work was the existence of an intermediate regime region observed between the quasi-static and rapid granular regimes, where the shear stress depends on the shear rate as a power law with an exponent ranging from zero to two, both with and without aeration. This intermediate regime was also observed in the work proposed by Langroudi et al.[28] where glass beads (0.1, 0.5, and 1 mm diameter) were subjected to shearing in a Couette flow configuration. In such work, no aeration was involved, and the Couette configuration was modified in order to let the particles flow vertically by gravitational effect in a continuous way. Experiments with and without vertical flow were performed. The results without vertical flow showed that increasing the shear rate does not result in any significant variation in the shear stress, which indicates that the material remains in the frictional, quasi-static regime. However, when the vertical flow is allowed, the results showed two distinct regimes: a quasi-static regime (at low shear rates) and an intermediate regime where the shear stress increases as the shear rate increases.

The studies discussed show that aerated shearing devices, such as the aerated coaxial cylinder viscometer,[4,9,16,26-29,31] have the potentials to shed light on the flow behavior of granular materials in some relevant flow regimes.

The main objective of this work is to develop a rheometer based on the coaxial cylinder viscometer flow configuration that confirms and expands previous studies on the shear stresses that develop in granular materials when they are aerated. To undertake such

experimental campaign, a three-dimensional (3D) geometry, composed of six blades, similar to the one developed by Marchal et al.,[6] was adapted to the Freeman FT4 powder rheometer aeration kit. The new 3D printed cell rotates at a fixed position inside the studied aerated material in a virtual Couette flow-type configuration, where the inner rotating cylinder is a virtual cylinder of particles comprised between the blades of the rotating cell. The shear stress and shear rate are computed from the recorded torque and rotational velocities, respectively, using the equations proposed by Ait-Kadi et al.[32] Those equations are obtained considering the existence of an optimal radial position, r^*, where both the shear rate and the shear stress are independent of the cell geometry, which was confirmed for various Newtonian and non-Newtonian fluids.[32]

In the present study, we verify first the applicability of the concept of the optimal radius r^*, when shearing granular materials, by testing five different 3D printed geometries (two heights and three radiuses). The cells were tested with a Newtonian fluid (glycerol 99%) of known viscosity, then nonaerated glass beads (of three different sizes) were used; those powders are known to exhibit Coulomb flow behavior in the quasi-static regime.[6] The powders were then aerated with an aeration ratio U/U_{mf} ranging from 0 to 0.4. Most of these measurements fell into the quasi-static regime and only a limited number of measurements fell into the intermediate regime. Subsequently, the measurements were compared to the constitutive law proposed by Jop et al.[17] for a final qualitative validation.

2 | EXPERIMENTAL APPARATUS

The aerated bed virtual Couette rheometer (AB-VCR) consists of the combination of the aeration vessel of the automated Freeman FT4 Powder Rheometer (Freeman Tech.) and a cylindrical cell displaying six blades as shown in Figure 1a,b. The aerated vessel of the FT4 is made of a 25 mm inner radius (R_e: external radius of the Couette configuration) glass cylinder that can hold a volume up to 260 ml. Two 50 mm diameter attachments can be used as a base for the glass vessel bottom: a plastic base (Figure 1c) for tests with liquids, and an aeration stainless steel base for aerated granular material tests (Figure 1c′). The latter is composed of a grid that allows for a uniform distribution of the injected air at ambient conditions throughout the cross section. The air flowing through the vessel is controlled by the FT4 air supply that assures air velocities up to 40 mm/s. In this study, five cylindrical cells of different geometries, as reported in Table 1, were designed and 3D printed using plastic material (ABS-M30i—provided by SYS systems 3D Printing).

The experimental procedure is as follows: the cell moves downward through the material placed in the vessel until it reaches a fixed position, which, in the present study, is assumed to be constant and equal to 1 mm, measured from the bottom of the vessel. The granular material under investigation is first fluidized at high airflow to allow the cell to move downward; this to avoid that the cell compacts the sample and causes the device to be overloaded. Once the cell has reached the fixed position, the aeration is stopped and the arm holding the cell starts rotating at a fixed rotational speed, ω. The vessel is filled with enough material to cover the height of each studied cell. The rotational movement of the cell creates a virtual rotating cylinder of particles comprised between the blades. The torque, T, needed to rotate this cylinder of particles through the remaining bed of particles is recorded. This procedure is followed while aerating the granular bed from the bottom. The models used to compute the shear stress and shear rates from the recorded torques and the rotational speeds are presented in the section below.

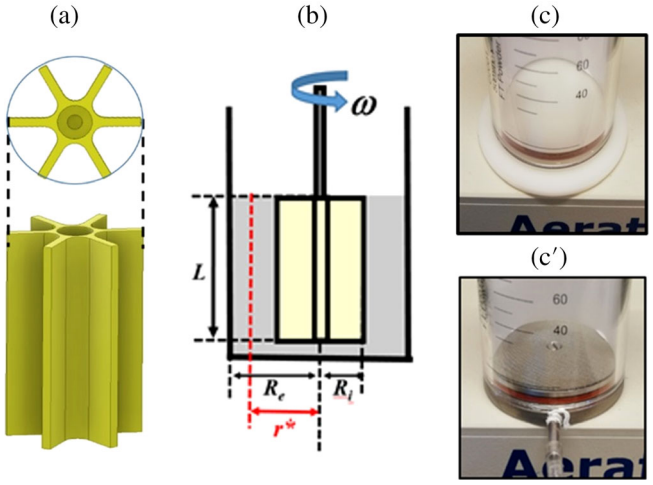

FIGURE 1 (a) Representative image of the 3D printed virtual Couette cell. (b) Schematic view of the assembled aerated bed virtual Couette rheometer (AB-VCR) with L being the cell's height, ω the rotational speed, R_e, R_i, and r^* the external, inner, and optimal radii, respectively. (c,c′) plastic and aeration base [Color figure can be viewed at wileyonlinelibrary.com]

TABLE 1 Dimensions and optimal position r^* of the 3D printed cells. R_e, R_i, and L are defined in Figure 1. The values of r^* are evaluated using Equation (4)

R_e (mm)	Height L (mm)	R_i (mm)	r^* (mm)	Name
25	70	18	20	Cell-1
		15	17.1	Cell-2
		10	11.6	Cell-3
25	20	18	20	Cell-4
		15	17.1	Cell-5

2.1 | Evaluation of the shear rate and shear stress

The shear rate, $\dot{\gamma}$, and shear stress, τ, are computed from the rotational speed, ω, and the recorded torque, T, as follows:

$$\tau = K_\tau(r)T \quad \text{with} \quad K_\tau(r) = \frac{1}{2\pi L r^2} \tag{2}$$

$$\dot{\gamma} = K_{\dot{\gamma}}(r,n)\omega \quad \text{with} \quad K_{\dot{\gamma}}(r,n) = (2/n)\frac{(R_e/r)^{2/n}}{(R_e/R_i)^{2/n}-1} \tag{3}$$

where n is the flow index and $K_\tau(r)$ and $K_{\dot\gamma}(r,n)$ are the shear stress and shear rate geometrical constants, respectively. These constants are obtained by solving the equation of motion in the case of a fluid obeying a power law model ($\tau = \upsilon\dot\gamma^{\,n}$) in a Couette flow configuration, where the boundary conditions are imposed by the internal (R_i) and external (R_e) radii. It should be noted that Equation (2) is obtained while considering a uniform stress distribution along the height of the cell, L. The solution of Equation (3) shows the dependence of $K_{\dot\gamma}$ on the flow index, n. Ait-Kadi et al.[32] proved that there is an optimal radial position r^* (Figure 1b) where $K_{\dot\gamma}$ is independent of n. This position corresponds to the intersection point of the curves $K_{\dot\gamma}(r)$ when evaluated at different values of the flow index, n. Figure 2 shows an example of the evolution of $K_{\dot\gamma}$ as a function of the position r obtained in the present work (Cell-1), with a flow index, n, varying from 0.15 to 1.

Figure 2 shows that a radial position ($r^* \approx 20$ mm) exists, which corresponds to the intersecting point between all the presented curves, where $K_{\dot\gamma}$ is independent of the flow index, n. This position can be evaluated analytically by solving the equation $K_{\dot\gamma}(n) = K_{\dot\gamma}(n')$, where n and n' are two different values of the flow index. The solution of the previous equation leads to the following relation[32]:

$$r^* = \left[\frac{n'}{n} \times \frac{(R_e/R_i)^{(2/n')} - 1}{(R_e/R_i)^{(2/n)} - 1} \times R_e^{(2/n - 2/n')}\right]^{(1/(2/n - 2/n'))} \tag{4}$$

To cover a large range of shear-thinning behaviors, two different values of n and n' need to be selected, for instance, $n = 1$ and $n' = 0.15$. It has been shown that closer n and n' values are more accurate is the determination of r^*.[32] Consequently, as long as K_τ and $K_{\dot\gamma}$ are evaluated at the optimal position, r^*, they can be considered as geometrical constants independent of n. The shear rate and stress, at r^*, can be easily evaluated by rewriting Equations (2) and (3):

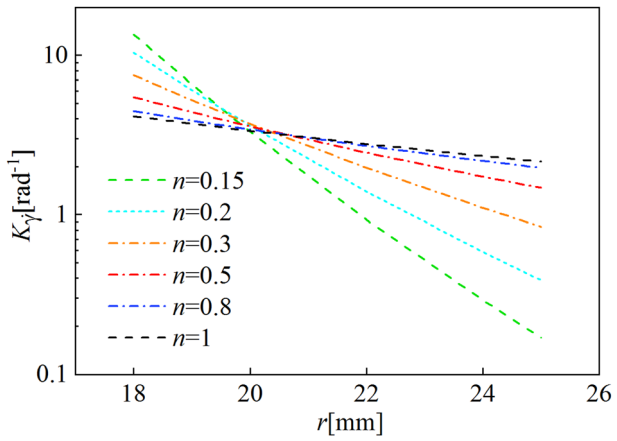

FIGURE 2 Shear rate geometrical constant, $K_{\dot\gamma}$, as a function of the radial position, r, in Cell-1 (see Table 1 for cell geometry) for various flow indexes, n. Optimal radial position $r^* \approx 20$ mm [Color figure can be viewed at wileyonlinelibrary.com]

$$\tau = \frac{1}{2\pi L r^{*2}} T \tag{5}$$

$$\dot\gamma = 2\frac{(R_e/r^*)^2}{(R_e/R_i)^2 - 1}\omega \tag{6}$$

The existence of r^* was confirmed experimentally by Ait-Kadi et al.[32] while performing several experiments using standard and non-conventional Couette geometries to measure the viscosity of known Newtonian and non-Newtonian fluids. The results showed that, when evaluated at the optimal radial position, r^*, the viscosities measured were in good agreement with their known values, independently of the device geometry. For the present study, r^* was evaluated using Equation (4), this with n and n', respectively, equal to 1 and 0.15; all the other geometrical values of the cells are evaluated and presented in Table 1.

2.2 | Experimental validation of the AB-VCR

Prior to performing shear tests on an aerated granular material bed, the AB-VCR was tested with a Newtonian liquid of known viscosity (glycerol). It was also tested with three different glass bead powders, which are known to behave as a Coulomb fluid in the quasi-static regime,[6] where the viscosity is inversely proportional to the shear rate. For these measurements, various cells geometries were tested to verify the applicability of Equations (5) and (6) to granular materials.

2.3 | Viscosity measurement of a Newtonian liquid

Glycerol (99% purity and viscosity 1.4 Pa/s) was initially tested. Four 3D printed cells were employed with a rotational speed varying from 5 to 70 rpm. For each fixed rotational speed, the torque was recorded for 60 s. Illustrative examples of the time evolution of the torque are presented in Figure 3.

Figure 3 shows that for all geometries and rotational speeds, the recorded torque is steady in time with some variations observed at very low rotational speeds (Figure 3b,b′). Nevertheless, the highest variation observed for these recorded torques does not exceed 11%. This graph also shows that the recorded torques vary with the cell geometries. Indeed, for a fixed rotational speed and a fixed radius, the recorded torque decreases as the cell height decreases. The same behavior is observed when decreasing the radius with a fixed cell height. Such behavior is expected, as the forces involved in moving the fluid vary with the cell surface area. Equation (5) is then used to compute the shear stresses from the recorded torques. Subsequently, the average values, over the last 40 s measurements, were evaluated for each geometry. The highest standard deviation (SD), between the 40 s measurements was found to be equal to 0.06 Pa which represents 0.2% of the highest evaluated shear stress. The rotational speeds were used to compute the shear rates using Equation (6). The shear stress for glycerol is represented as a function of the shear rate for various cell geometries in a linear scale in Figure 4a and a log–log scale in Figure 4b. The theoretical values

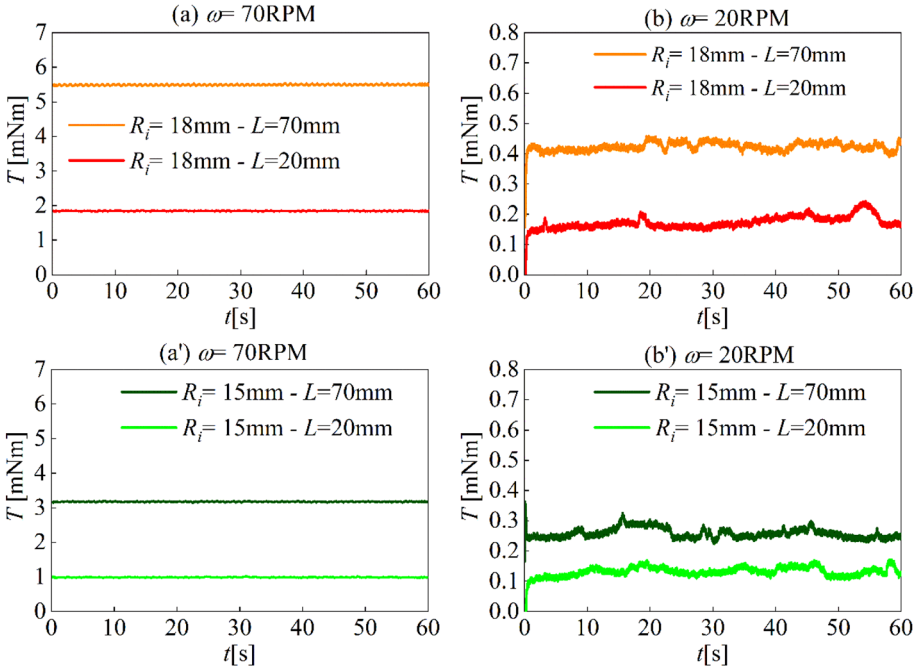

FIGURE 3 Time evolution of the recorded torque for glycerol. The results are obtained with four geometries: (a,b) Cell-1 and Cell-4. (a′,b′) Cell-2 and Cell-5. (The graphs on the left are obtained at 70 rpm and the ones on the right at 5 rpm) [Color figure can be viewed at wileyonlinelibrary.com]

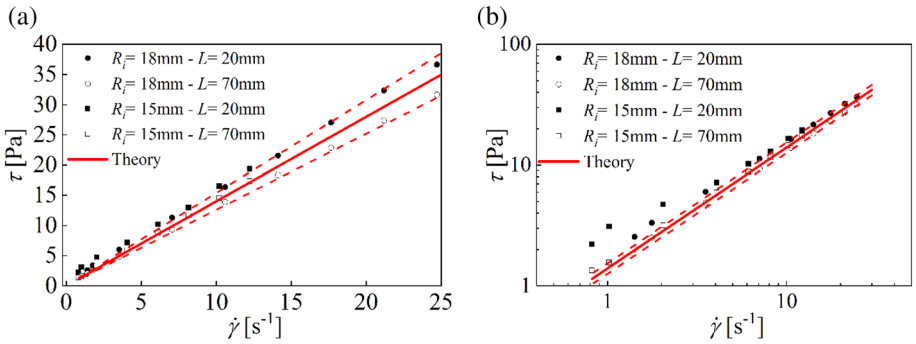

FIGURE 4 Shear stress as a function of the shear rate, for the four cells tested with glycerol 99%. The red solid line refers to theoretical values (υ = 1.4 Pa/s) and the dashed lines refer to ± 10% confidence interval from the theoretical value [Color figure can be viewed at wileyonlinelibrary.com]

obtained with the known viscosity of the glycerol are also plotted in the same graph (red solid line), showing a variation of ±10% (red dashed lines).

It can be seen from Figure 4a,b that for all studied cells, the shear stress increases proportionally with the imposed shear rate, following the equation $\tau = \upsilon\dot{\gamma}$, which is the characteristic curve of a Newtonian fluid. Furthermore, it should also be noted that the experimental shear stresses are in good agreement with the theoretical line (solid red) corresponding to the known viscosity value. However, the measured viscosity shows discrepancy as the shear rate becomes lower than 1 s^{-1} for Cells 4 and 5. It appears that the best agreement with the theoretical value is found to be for Cell-1 (L = 70 mm and R_i = 18 mm) and Cell-2 (L = 70 mm and R_i = 15 mm); hence, those two cells will be used for the glass beads measurements presented in the following.

2.4 | Glass beads powder measurements

The AB-VCR was tested with dry, noncohesive spherical glass beads with three different size distributions: a monodispersed sample with particle diameter $d_{p\text{-}1}$ = 0.5 mm and two polydispersed samples with diameters $d_{p\text{-}2}$ ranging from 0.05 to 0.08 mm and $d_{p\text{-}3}$ ranging from 0.16 to 0.21 mm. The particles size ranges were obtained by mass distribution and will be referred to as $d_{p\text{-}2}$ = 0.05–0.08 mm and $d_{p\text{-}3}$ = 0.16–0.21 mm. Those glass beads were chosen in order to isolate the flow behavior from the possible effect of variables such as the particles morphology or surface interaction. The steady-state friction coefficient, μ_s, of particles with diameter $d_{p\text{-}1}$ was evaluated in a previous study[34] using the FT4 shear stress experiments. The same methodology was used for the evaluation of the friction coefficient for $d_{p\text{-}2}$ and $d_{p\text{-}3}$ particles and the corresponding values are reported in Table 2.

The three glass bead samples were then tested using Cell-1, Cell-2, and Cell-3 to verify the applicability of Equation (5) in granular materials. The rotational speeds for each cell were fixed as follows: from 62 to 8 rpm for Cell-1, from 87 to 11 rpm for Cell-2 and from 120 to 15 rpm for Cell-3. Those rotational speeds were chosen according to Equation (6) in order to shear the powders at the same shear rates varying from 22 to 2.75 s^{-1}. For each of the studied rotational speed, the torque needed to move the cell through the bed of

FI (–)	μ_s (FT4)	U/U_{mf} (mm/s)	τ_{av} (Pa)	*P* (Pa)	*P** = PA/mg (–)
$d_{p\text{-}1}$ (0.5 mm)					
0	0.46 ± 0.02	0	235 ± 2	512	0.5
0.1		20.5/205	197 ± 4	429	0.42
0.2		41/205	175 ± 3	380	0.38
$d_{p\text{-}2}$ (0.05–0.08 mm)					
0	0.36 ± 0.01	0	282.5 ± 2	716	0.71
0.1		0.38/3.8	226.1 ± 1.9	628	0.63
0.2		0.76/3.8	199.7 ± 1.1	524	0.52
0.3		1.14/3.8	160 ± 1.9	427	0.43
0.4		1.52/3.8	118.9 ± 0.8	344	0.34
$d_{p\text{-}3}$ (0.16–0.21 mm)					
0	0.32 ± 0.01	0	260 ± 4.8	858	0.87
0.1		2.95/29.5	228.4 ± 4.2	690	0.69
0.2		5.90/29.5	190.6 ± 3.2	605	0.61
0.3		8.85/29.5	155.9 ± 2.2	483	0.49
0.4		11.8/29.5	125.9 ± 1.9	360	0.36

TABLE 2 Average shear stress, τ_{av}, and pressure, *P*, calculated at various *FI*. μ_s is the steady-state friction coefficient, *U* and U_{mf} are the air and the minimum fluidization velocities, respectively. *P** is the pressure normalized with the sample weight

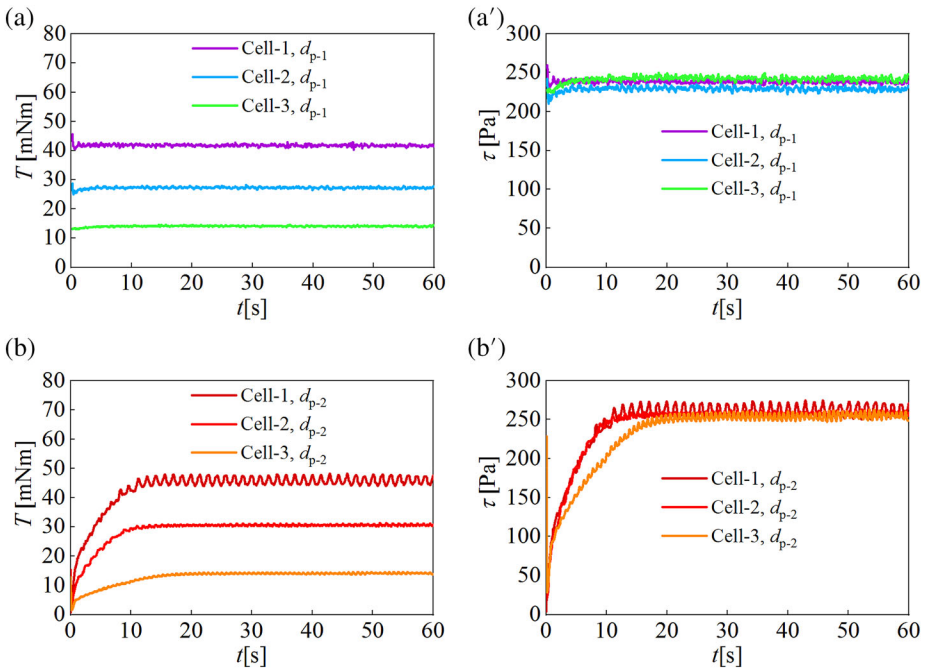

FIGURE 5 Time evolution of recorded torques (a,b) and the corresponding shear stresses (a′,b′) at shear rate equal to 14.7 s^{-1} with $d_{p\text{-}1}$ = 0.5 mm and $d_{p\text{-}2}$ = 0.05–0.08 mm. The shear stress is evaluated by Equation (5). See Table 1 for the cell geometries [Color figure can be viewed at wileyonlinelibrary.com]

particles was recorded for 60 s. Examples of the recorded torques obtained at a shear rate equal to 14.7 s^{-1}, together with the corresponding shear stresses evaluated with Equation (5), are presented in Figure 5. Similar measurements as the one presented in Figure 5 were performed at different rotational speeds but are not presented here.

Figure 5a,b highlights that all the recorded torques reach a steady value after a certain time (t > 10 s), this regardless of particles size and studied cells. For a fixed particle size, a variation in the recorded torque between the three studied cells can be observed in Figure 5a,b. This variation is expected, as the forces involved in moving the powder vary according to the cell surface area. As the shear stresses are computed using Equation (5), the measured values collapsed to a same value that is independent of the cell geometries (see Figure 5a′, b′). The evaluated shear stresses are then averaged over the last 40 s for all the studied cells and at various shear rates. The evolution of the resulting shear stress, as a function of the shear rate, are presented for the three cells and particles with diameters of $d_{p\text{-}1}$ (Figure 6a) and $d_{p\text{-}2}$ (Figure 6b).

Figure 6 shows a good agreement between the evaluated shear stresses for various cells with a fixed particle size. These observations confirm the applicability of Equation (5) for evaluating the shear stress

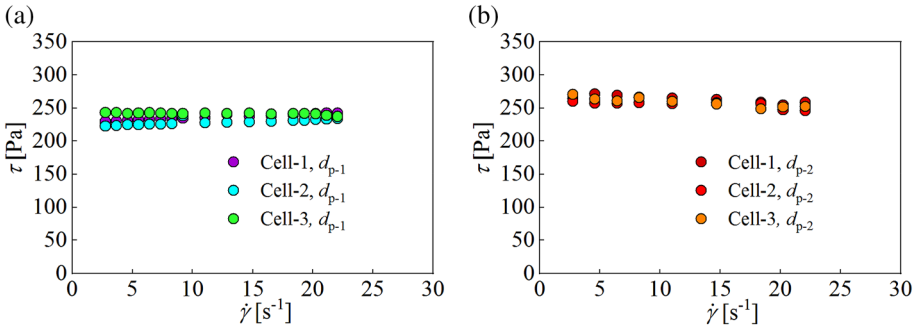

FIGURE 6 Evolution of shear stress as a function of shear rate obtained with various cells for particles with diameters: (a) d_{p-1} = 0.5 mm and (b) d_{p-2} = 0.05–0.08 mm. See Table 1 for the cell geometries [Color figure can be viewed at wileyonlinelibrary.com]

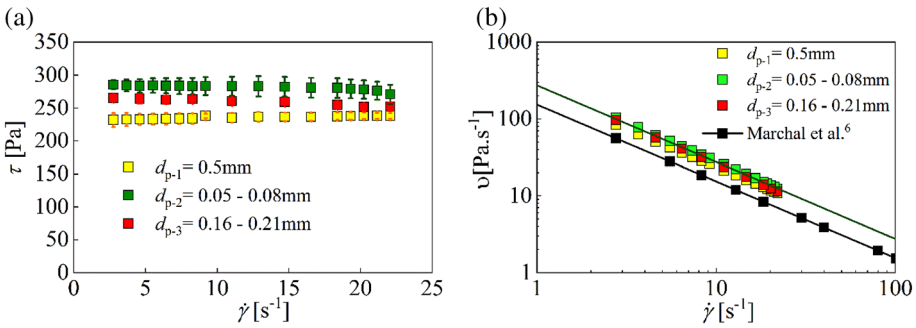

FIGURE 7 Shear stress (a) and viscosity (b) as a function of shear rate. The error bars correspond to the *SD* of the geometry dependency [Color figure can be viewed at wileyonlinelibrary.com]

of a granular material which is not dependent on the cell radius. For each studied glass beads, the shear stresses obtained with the different cells are averaged, and the corresponding results are presented in Figure 7. The error bars correspond to the *SD* which is consequent of the cell geometry.

The results presented in Figure 7a show that for all three studied powders the shear stress is independent of the shear rate. These results also point out that there is no correlation between the shear stress and the particle size. Lower shear stress values are obtained with the largest studied particles (d_{p-1} = 0.5 mm), while higher values are obtained with d_{p-3} = 0.16–0.21 mm. The shear stresses for the smallest particles with diameter d_{p-2} are in between powders of diameter d_{p-1} and d_{p-3}. This variation might be explained by the difference in the friction coefficients of the studied samples (Table 2). Also, for a fixed shear rate, the shear stress increases as the friction coefficient decreases. Additional experiments were carried out to study the effect of the 1 mm gap between the 3D printed cell and the bottom of the vessel on the experimental measurements. The gap distance was varied from $3d_p$ to $150d_p$; no variation of the shear stress measurements was recorded.

The solid viscosities are evaluated as the ratio of shear stress to shear rate and the results are plotted in Figure 7b. The viscosities for 0.53 mm diameter glass beads, measured by Marchal et al.,[6] are also plotted in the same graph. The viscosity decreases with increasing the shear rate (Figure 7b) following a power law fit with slope equal to −1. This corresponds to a Coulomb behavior which was also observed by Marchal et al.,[6] using a similar cell configuration. The results presented in Figure 7b also show that the viscosity is independent of the particle size. There is a slight variation between the different measurements, which indicates that the evaluated viscosity depends on the material. It has been shown previously that the shear stress measurements are independent of the radius (Figure 6). Figure 7b shows differences between the present study and the work by Marchal et al.,[6]; given that the particles used in the two studies are made of the same material, it is speculated that the variation observed Figure 7b might be explained by the difference in the height *L* of the cells used in the two studies (*L* = 30 mm in Marchal et al.[6]). Indeed, Equation (5) is applied while assuming a uniform stress distribution along the height *L*, which might not be the case in granular materials.

2.5 | Aerated bed

Prior to perform shear tests with aeration, the AB-VCR was tested to determine to what extent, if any, the rotational speed of the inner cell altered the basic fluidized bed characteristics. To do so, the FT4 aeration vessel was used as a fluidized bed without cell where particles d_{p-2} and d_{p-3} were tested. The same fluidized bed configuration with Cell-2 was used to perform measurements at two rotational speeds (4 and 20 rpm). In Figure 8, the FI = ΔPA/mg is shown as a function of the normalized air velocity, U/U_{mf}, where A is the aerated surface area, m is the total mass of particles in the bed (200 g), U is the air velocity, and U_{mf} is the minimum fluidization velocity. The latter is evaluated experimentally from the fluidized bed tests performed with d_{p-2} and d_{p-3} particles and the corresponding values are presented in Table 2. A theoretical line, representing the perfect equilibrium where FI is equal to the ratio U/U_{mf} $FI = U/U_{mf}$, is also plotted in Figure 8 as reference (solid red line). The good agreement found between the

results with and without cell for both particle sizes and both rotational speeds (Figure 8) indicates that having the cell rotating inside the aerated bed does not have a strong effect on its fluidization behavior. However, it should be noted that a deviation from the linear behavior of the fixed bed is observed with the sample $d_{p\text{-}2}$, obtained without the use of the cell. We attribute this deviation to the small size of the particles, which are cohesive and therefore more difficult to fluidize. Indeed, the results show that the deviation decreases when the VCC is used, which indicates that the presence of the cell increases the flowability of the sample. The same comment about the effect of the VCC on the flowability can be made for $FI > 1$.

For the present study, the same experimental procedure presented previously in the experimental validation section is repeated with air flowing through the bottom of the cell. The three cells (1–3, and) and the three glass bead samples ($d_{p\text{-}1}$, $d_{p\text{-}2}$, and $d_{p\text{-}3}$) used previously, were used in these experiments as well. The air velocities were adjusted according to the particles size in order to perform experiments at the same *FI*. The air velocities used in this study, together with U_{mf} and the corresponding *FI*, are reported in Table 2. The shear tests were performed for a shear rate ranging from 22 to 2.75 s^{-1} with four values of *FI* for $d_{p\text{-}2}$ and $d_{p\text{-}3}$ particles (0.1, 0.2, 0.3, and 0.4). For $d_{p\text{-}1}$ particles, U_{mf} was estimated theoretically[35] given that its value was higher than the maximum air velocity supported by the FT4 (40 mm/s). Therefore, the shear tests were only performed with two values of *FI* (0.1 and 0.2). For the three studied cells and for each shear rate, particle size, and *FI*, the torque was recorded for 60 s and it was found to be steady in time for all cases. The shear stress was then computed using Equation (5) and averaged over the last 40 s. Good agreement was found between the results with different cells for one size of particle and one *FI*. For each size of particle and *FI*, the shear stresses obtained with three different cells, are averaged and the corresponding results are presented as a function of the shear rate in Figure 9 (only $d_{p\text{-}2}$ and $d_{p\text{-}3}$ are shown), where the error bars correspond to the *SD* of the cell geometry dependency.

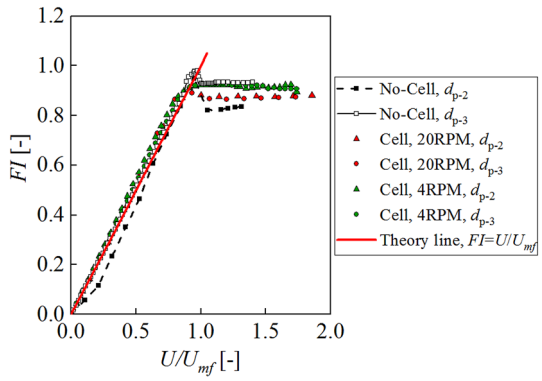

FIGURE 8 Comparison of the fluidization curves obtained with and without aerated bed virtual Couette rheometer (AB-VCR). Only Cell-2 was used for this measurement with two rotational speeds and two particle sizes ($d_{p\text{-}2}$ = 0.05–0.08 mm and $d_{p\text{-}3}$ = 0.16–0.2 mm). The solid red line is a theoretical line representing the perfect equilibrium $FI = U/U_{mf}$ [Color figure can be viewed at wileyonlinelibrary.com]

The results presented in Figure 9 show that when the particles are aerated, good agreement is found between the shear stresses obtained using different cells, and negligible *SD* between the cells measurements is recorded (highest value around ±20 Pa which represents ±8% of the corresponding shear stress observed with $d_{p\text{-}3}$ particles with $FI = 0.2$). In Figure 9 it can be seen that the shear stress decreases as *FI* increases. This might be explained by the fact that when aerated, the pressure acting on the particles decreases, which leads to a decreasing in viscosity. However, for a fixed shear rate, the shear stress decreases in a nonlinear way with increasing *FI* and an extrapolation of the results will lead to a shear stress equal to 0 for values of *FI* below 1, which is unlikely to happen. This observation might indicate that the studied powder will no longer be in the frictional quasi-static regime even if the aeration velocity is below U_{mf} and one can assume that the transition to an intermediate regime will occur for $FI < 1$. The graphs presented Figure 9 also show that for all the studied *FI* and particle sizes, the shear stress in the aerated bed is independent of the studied shear rates, describing the Coulomb behavior observed without aeration (Figure 7). It should be noted that the same behaviors were observed with $d_{p\text{-}1}$ particles (not shown in Figure 9). The average shear stress over the studied shear rates is evaluated for each *FI* and each particle size, and the corresponding values are reported in Table 2. For all studied $FI > 0$, good agreement is found between the average shear stresses, τ_{av}, obtained for particles of diameters $d_{p\text{-}2}$ and $d_{p\text{-}3}$, this even if the air velocity, *U*, was different. The shear stresses for particles of diameter $d_{p\text{-}1}$ are systematically lower than the one obtained with the other two powders. This might be explained by the different friction coefficient of the studied powders. Indeed, the FT4 shear stress analysis showed that the value of the steady-state friction coefficient, μ_s, of $d_{p\text{-}1}$ particles is found to be around 0.46 while the one for $d_{p\text{-}2}$ and $d_{p\text{-}3}$ particles are found to be around 0.36 and 0.32, respectively.

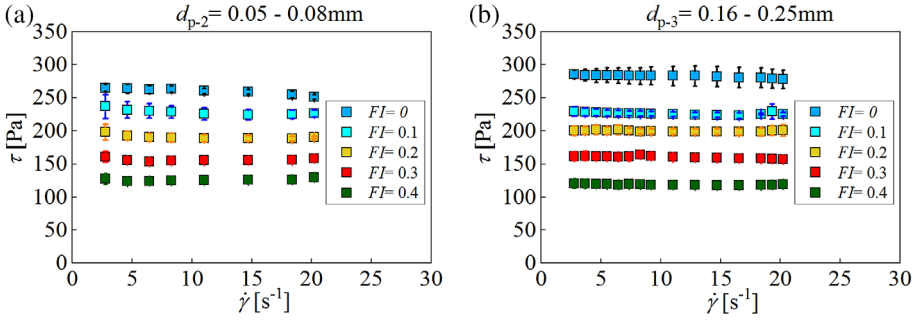

FIGURE 9 Shear stress as a function of shear rate at various FIs: (a) $d_{p\text{-}2}$ = 0.05–0.08 mm and (b) d_{p3} = 0.16–0.21 mm. The air velocities corresponding to each *FI* are reported Table 2. The error bars correspond to the *SD* of the cell geometry dependency [Color figure can be viewed at wileyonlinelibrary.com]

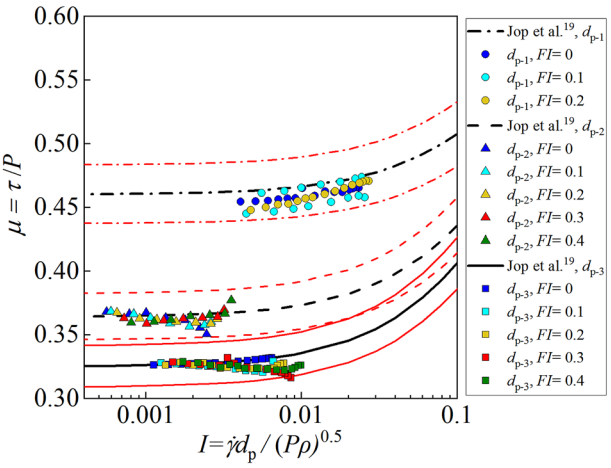

FIGURE 10 Comparison between the measured coefficients of internal friction and those predicted by the model proposed by Jop et al.[17] The red lines correspond to a model variation of ±5% [Color figure can be viewed at wileyonlinelibrary.com]

2.6 | Constitutive law: qualitative validation

In this session, the experimental results are modelled based on the constitutive law proposed by Jop et al.,[17] (Equation (1)). The experiments are assumed to be performed in the quasi-static regime (I < 0.01) where μ_s is independent of the shear rate. Therefore, the pressure P, which is assumed to be constant for each FI, is estimated as the ratio of the average shear stress, τ_{av}, to the steady-state friction coefficient, μ_s. The values of the estimated pressures are reported in Table 2 together with the normalized pressure P^* = PA/mg. For all studied values of FI, the estimated pressure is always lower than the sample weight, this with P^* being systematically lower than 1.

The graph plotted in Figure 10 shows the comparison between the measured $\mu(I)$, which were evaluated using the estimated P, and the one evaluated with the constitutive law (Equation (1)), where μ_2 and I_0 were taken as typical values for glass beads proposed in the literature[36] and are equal to 0.65 and 0.3, respectively. The plotted models are all presented with a variation of ±5% (red lines).

The results presented in Figure 10 show that for an inertial number lower than 0.003, good agreement is found between the measured $\mu(I)$, obtained for d_{p-2} and d_{p-3} particles, and the one predicted by the model independently of FI. For inertial numbers higher than 0.003, the model overestimates the measured $\mu(I)$ for both d_{p-1} and d_{p-3} particles and for all the studied values of FI. However, the discrepancy between model and the experimental values, in this range of inertial numbers, does not exceed 5% and the shape of the experimental curve follows the shape of theoretical one with $\mu(I)$ increasing as the inertial number increases. One should bear in mind that the experimental results presented in Figure 10 are obtained with an estimated value of the pressure, which might not be the real one. Nevertheless, these results validate qualitatively the methodology presented in this paper for the evaluation of the measurements of particle stresses in an aerated granular bed.

3 | CONCLUSIONS

In this study, a 3D printed cylindrical cell composed of six blades was adapted to the aeration kit of the Freeman FT4 rheometer in order to perform shear test experiments on aerated powders in a Couette flow configuration. This new rheometer prototype, named AB-VCR, was developed for the measurements of bulk solid stresses of granular material in an aerated bed. It was first validated with a Newtonian fluid (glycerol 99% of known viscosity) without aeration. The evaluated shear stress was found to be proportional to the applied shear rate describing the expected Newtonian behavior. The viscosity was found to be in good agreement with the theoretical value and independent of the geometry of the 3D printed cells. This prototype rheometer was also tested and validated for nonaerated glass bead powders (particle size ranging from 0.05 to 0.5 mm), where the shear stress was found to be independent of the applied shear rate (ranging from 3 to 22 s^{-1}), confirming the Coulomb behavior of the granular materials in the quasi-static regime.[6] Similar behavior was obtained for the three studied samples and showed to be independent of the cell radius. The shear stress was also found to increase when the friction coefficient decreases. The device was finally tested as an aerated bed rheometer by varying the velocity of the air injected through the three glass bead samples studied. The aeration velocities were chosen according to the minimum fluidization velocity of each sample, in order to ensure that the shear tests were performed on a fixed aerated bed (U/U_{mf} < 1). The main findings of the aerated bed measurements are summarized as follows:

For a fixed aeration velocity, U, the evaluated shear stress was found to be independent of the imposed shear rate (ranging from 3 to 22 s^{-1}) describing the Coulomb behavior observed without aeration for the three glass bead samples. The shear stress was also found to be decreasing with increasing the aeration velocity.

For a fixed FI, good agreement was found between the results obtained with samples having steady-state friction coefficients of similar value (*i.e.* μ_s = 0.33 and 0.36), while the shear stress obtained with the sample having a higher steady-state friction coefficient (μ_s = 0.46) was found to be systematically lower than the shear stress of the other two samples with lower friction coefficient.

Good agreement was found between the experimental $\mu(I)$, which was evaluated as the ratio of the shear stress, τ, to an estimated pressure P, and the one predicted by the model proposed by Jop et al.,[17] for all studied FI and particle sizes.

ACKNOWLEDGMENT

Financial support from the EPSRC (grant no. EP/N034066/1) is kindly acknowledged.

NOTATION

d_p particle diameter
FI fluidization index

I	inertial number
I_0	constant in Equation (1)
K	geometrical factors (rad^{-1})
L	cell height (m)
n	flow index
P	pressure (Pa)
r	radial position (m)
r^*	optimal radial position (m)
R_i	inner radius (m)
R_e	external radius (m)
t	time (s)
U	air velocity (m/s)
U_{mf}	min fluidization velocity (m/s)

GREEK

τ	shear stress (Pa)
$\dot{\gamma}$	shear rate (s^{-1})
υ	viscosity (Pa/s)
ρ	particle density (kg/m^3)
ω	rotational speed (rpm)
μ	coefficient of internal friction
μ_s	coefficient of internal friction at low I
μ_2	coefficient of internal friction at high I

ORCID

Raffaella Ocone https://orcid.org/0000-0003-4895-9627

REFERENCES

1. Muzzio FJ, Alexander A, Goodridge C, Shen E, Shinbrot T. Solids mixing part A: fundamentals of solids mixing. In: EL Paul, VA Atiemo-Obeng, SM Kresta Eds, *Handbook of Industrial Mixing: Science and Practice*; Wiley, New Jersey, 2004:887-985.
2. Schaeffer DG. Instability in the evolution equations describing incompressible granular flow. *J Differen Equat*. 1987;66:19-50.
3. Prevost JH. A simple plasticity theory for frictional cohesionless soils. *Int J Soil Dynam Earthq Eng*. 1985;4:9-17.
4. Anjaneyulu P, Khakhar DV. Rheology of a gas-fluidized bed. *Powder Technol*. 1995;83:29-34.
5. Schwedes J. Review on testers for measuring flow properties of bulk solids. *Granul Matter*. 2003;5:1-43.
6. Marchal P, Smirani N, Choplin L. Rheology of dense-phase vibrated powders and molecular analogies. *J Rheol*. 2008;53:1-29.
7. Leturia M, Benali M, Lagarde S, Ronga I, Saleh K. Characterization of flow properties of cohesive powders: a comparative study of traditional and new testing methods. *Powder Technol*. 2014;253:406-423.
8. Louati H, Oulahna D, de Ryck A. Effect of the particle size and the liquid content on the shear behavior of wet granular material. *Powder Technol*. 2017;315:398-409.
9. Tardos GI, Khan MI, Schaeffer DG. Forces on a slowly rotating, rough cylinder in a Couette device containing a dry, frictional powder. *Phys Fluids*. 1998;10:335-341.
10. Garzó V, Dufty JW. Dense fluid transport for inelastic hard spheres. *Phys Rev E*. 1999;59:5895-5911.
11. Johnson PC, Jackson R. Frictional–collisional constitutive relations for granular materials, with application to plane shearing. *J Fluid Mech*. 1987;176:67-93.
12. LaMarche CQ, Liu P, Kellogg KM, Hrenya CM. Fluidized-bed measurements of carefully-characterized, mildly-cohesive (group a) particles. *Chem Eng J*. 2017;310:259-271.
13. Xu H, Zhong W, Shao Y, Yu A. Experimental study on mixing behaviors of wet particles in a bubbling fluidized bed. *Powder Technol*. 2018;340:26-33.
14. Pang L, Shao Y, Zhong W, Liu H. Experimental investigation on the coal combustion in a pressurized fluidized bed. *Energy*. 2018;165:1119-1128.
15. Guo L, Wang Z, Zhong S, Bao Q, Guo Z. Fluidization state monitoring using electric current during fluidized bed reduction of iron ore. *Powder Technol*. 2019;343:683-692.
16. Colafigli A, Mazzei L, Lettieri P, Gibilaro L. Apparent viscosity measurements in a homogeneous gas-fluidized bed. *Chem Eng Sci*. 2009;64:144-152.
17. Jop P, Forterre Y, Pouliquen O. A constitutive law for dense granular flows. *Nature*. 2006;441:727-730.
18. MiDi GDR. On dense granular flows. *Eur Phys J E*. 2004;14:341-365.
19. Klein J, Höhne D, Husemann K. The influence of air permeation on the flow properties of bulk solids. *Chem Eng Technol*. 2003;26:139-146.
20. Barletta D, Donsì G, Ferrari G, Poletto M. A rotational tester for the characterization of aerated shear flow of powders. *Part Part Syst Char*. 2007;24:259-270.
21. Manuel Valverde J, Castellanos A, Ramos A, Pérez AT, Morgan MA, Keith Watson P. An automated apparatus for measuring the tensile strength and compressibility of fine cohesive powders. *Rev Sci Instrum*. 2000;71:2791-2795.
22. Castellanos A, Valverde JM, Quintanilla MAS. The Sevilla powder tester: a tool for characterizing the physical properties of fine cohesive powders at very small consolidations. *KONA Powder Part J*. 2004;22:66-81.
23. Peschl IASZ. Quality control of powders for industrial application. Proceedings of 14th annual Powder & Bulk Solids Conference, Chicago, IL. 1989; 517–536.
24. Bruni G, Barletta D, Poletto M, Lettieri P. A rheological model for the flowability of aerated fine powders. *Chem Eng Sci*. 2007;62:397-407.
25. Tomasetta I, Barletta D, Lettieri P, Poletto M. The measurement of powder flow properties with a mechanically stirred aerated bed. *Chem Eng Sci*. 2012;69:373-381.
26. Salehi H, Sofia D, Schütz D, Barletta D, Poletto M. Experiments and simulation of torque in Anton Paar powder cell. *Part Sci Technolgy*. 2018;36:501-512.
27. Tardos GI, McNamara S, Talu I. Slow and intermediate flow of a frictional bulk powder in the Couette geometry. *Powder Technol*. 2003;131:23-39.
28. Langroudi MK, Turek S, Ouazzi A, Tardos GI. An investigation of frictional and collisional powder flows using a unified constitutive equation. *Powder Technol*. 2010;197:91-101.
29. Landi G, Barletta D, Lettieri P, Poletto M. Flow properties of moisturized powders in a Couette fluidized bed rheometer. *Int J Chem React Eng*. 2012;10:1-13.
30. Schütz D, Riedl E, Romirer R, Hartmann K, Sack O. A multi-method approach to quality control illustrated on the industrial powder coating process. *Chem Eng Res Des*. 2018;139:136-143.
31. Lupo M, Schütz D, Riedl E, Barletta D, Poletto M. Assessment of a powder rheometer equipped with a cylindrical impeller for the measurement of powder flow properties at low consolidation. *Powder Technol*. 2019;357:281-290. https://doi.org/10.1016/j.powtec.2019.08.071.
32. Aït-Kadi A, Marchal P, Choplin L, Chrissemant A-S, Bousmina M. Quantitative analysis of mixer-type rheometers using the Couette analogy. *Can J Chem Eng*. 2002;80:1166-1174.

33. Martínez-Arias B, Peixinho J. Torque in Taylor–Couette flow of viscoelastic polymer solutions. *J Non-Newton Fluid Mech*. 2017;247:221-228.
34. Ait Ali Yahia L, Maione R, Ozel A, Ocone R. Numerical and experimental studies of granular materials in the quasi-static regime. 2018.
35. Wen CY, Yu YH. A generalized method for predicting the minimum fluidization velocity. *AIChE J*. 1966;12:610-612.
36. Pouliquen O, Cassar C, Jop P, Forterre Y, Nicolas M. Flow of dense granular material: towards simple constitutive laws. *J Stat Mech: Theory Exp*. 2006;2006:P07020.

How to cite this article: Yahia LAA, Piepke TM, Barrett R, Ozel A, Ocone R. Development of a virtual Couette rheometer for aerated granular material. *AIChE J*. 2020;66:e16945. https://doi.org/10.1002/aic.16945